CHIN. PHYS. LETT. Vol. 38, No. 3 (2021) 038101

Phase Stability and Hydroxyl Vibration of Brucite $Mg(OH)_2$ at High Pressure and High Temperature

Wei-Bin Gui(桂维彬), Chao-Shuai Zhao(赵超帅), and Jin Liu(刘锦)*

Center for High Pressure Science and Technology Advanced Research (HPSTAR), Beijing 100094, China

(Received 26 November 2020; accepted 28 December 2020; published online 2 March 2021)

Brucite $Mg(OH)_2$ is an archetypal hydrous mineral and it has attracted a great deal of attention. However, little is known about the evolution of hydroxyl groups in brucite with respect to subduction fluids. We carried out Raman measurements up to 15.4 GPa and 874 K via an externally heated diamond anvil cell, investigating the stability of brucite under the conditions relevant to subducting slabs. The hydroxyl vibration mode A_{1g}(I) of brucite is weakened under simultaneous high pressure-temperature conditions. Meanwhile, the presence of carbonated solution can destabilize the hydroxyl groups of brucite at low pressure. Our results suggest that brucite releases water when reacting with hydrogen carbonate ion to form magnesite $MgCO_3$ in subduction zones. This implies that the global water cycle is largely coupled with the deep carbon cycle in Earth's interior.

DOI: 10.1088/0256-307X/38/3/038101

Brucite $Mg(OH)_2$ is an important archetypal mineral for hydrous dense silicate minerals (HDSM) and the end-member component in the Mg–H–Si–O system in the deep Earth. It is formed during olivine-rich mantle hydration as a by-product of serpentinization reaction between olivine and water:[1]

$$2Mg_2SiO_4 + 3H_2O \rightarrow Mg_3Si_2O_5(OH)_4 + Mg(OH)_2.$$

This reaction implies that brucite may become an important component in the mantle wedge, and some petrology evidence indicates the existence of brucite up to 20 vol% in cold subduction zones.[2–5]

The physical and chemical properties of brucite have been extensively investigated at high pressure. The electronic conductivity of brucite increases by two orders of magnitude from 3.7 to 13 GPa at 450–750 K.[6] Moreover, brucite preferentially incorporates deuterium over hydrogen with increasing pressure, likely leading to an increasing D/H fractionation factor between brucite and water.[7] This indicates that the behavior of brucite in the deep Earth should be significantly different from that of surface environments. Furthermore, previous experimental and theoretical studies suggest that brucite could remain stable at high pressure up to 30 GPa under supercold subduction geothermal conditions.[8–11] With increasing pressure up to 30 GPa at room temperature, the Raman-active hydroxyl stretching vibration decreases at the rate of $\sim 7\,cm^{-1}$/GPa.[8] High temperature tends to make brucite decomposed into periclase (MgO) and H_2O. At ambient conditions, the decomposition temperature is around 674 K;[12,13] it increases to 1574 K at 11.5 GPa and the decomposition temperature then decreases with a ratio of −20 K/GPa above 11.5 GPa.[14] A kinetic study on brucite under high pressure-temperature (P–T) conditions showed that the dehydroxylation rate is positively correlated with temperature but decreases with increasing pressure.[15,16] These results indicate that the stability of brucite can be controlled by both pressure and temperature, whereas it remains unclear about the effects of high P–T on hydroxyl vibration of brucite. Due to the behavior of hydroxyl group reflecting the stability and dehydration of hydrous minerals, the Raman spectroscopy on hydroxyl vibration could thus be utilized to determine the stability of brucite under extreme conditions.

Regarding the stability of brucite in the deep Earth, most of the previous studies focused on the effects of pressure and temperature. However, the complex chemical compositions may also affect the stability of brucite in subduction zones. Experiments revealed that under the high P–T conditions, the solubility of calcite ($CaCO_3$) in aqueous solution dramatically increases, which results in HCO_3^--rich fluid through the following reaction:[17]

$$CaCO_3 + H^+ \rightarrow Ca^{2+} + HCO_3^-.$$

The hydrogen carbonate ion HCO_3^- is likely to react with the hydroxyl in brucite, which would influence the existence of brucite under the corresponding P–T conditions. To clarify the stability of brucite in subduction zones, we investigate how the hydroxyl vibration of brucite would change with or without the presence of HCO_3^- aqueous solution at the simultaneous high P–T conditions via Raman spectroscopy. These results provide new insights into the phase stability and hydroxyl evolution of brucite at the P–T conditions related to subduction zones.

Polycrystalline $Mg(OH)_2$ sample (CAS #1309-42-8) was commercially purchased from Alfa Aesar Chemical Company, Inc. For high-pressure experiments at room temperature, a symmetric diamond anvil cell (DAC) was applied, and the brucite pow-

Supported by the National Key Research and Development Program of China (Grant No. 2019YFA0708502).
*Corresponding author. Email: jin.liu@hpstar.ac.cn

der was placed in a 200-μm hole on a pre-indented T301 stainless gasket. For high P–T experiments, the external-heating DAC was used to generate high P–T environments, together with platinum (Pt) wire heater. Argon (Ar) was condensed by liquid nitrogen and loaded into the sample chamber as the pressure medium due to its clear Raman spectrum background at around 3600 cm^{-1}. To investigate the chemical stability of brucite in subduction fluids, brucite powder and 1 mol/L $NaHCO_3$ aqueous solution were chosen as starting materials. An Ar^+ laser at wavelength 532 nm (green) (Coherent Verdi V2) is used for *in situ* Raman spectroscopic measurements. The signal was collected using the Princeton Instrument PIXIS 400 with an 1800 G/mm ruled grating. The temperature was measured using a K-type thermocouple that was cemented to the anvil pavilion close to the tip of the diamonds, coupled with a temperature controller (Scistar-TC-1000, Beijing Scistar Technology Co., Ltd).

Brucite is a typical layered hydrous mineral of MgO_6 octahedral layer with hydrogen atoms between the interlayers.[18] In this study, the Raman spectrum of brucite at ambient conditions is illustrated in Fig. 1. The A_{1g}(I) mode corresponds to the hydroxyl vibration of brucite.[19] It was adopted to evaluate the frequency shifts of hydroxyl bands in brucite under the simultaneous high P–T conditions.

A ruby sphere in the diameter of 5–10 μm was placed next to brucite to determine the pressure in the sample chamber. The effects of temperature and pressure on ruby are assumed to be independent of each other within the P–T range of this study.[20,21] To determine the evolution of the ruby R_1 fluorescence with increasing temperature for the ruby used in this study, we collected a series of fluorescence spectra of the ruby R_1 line up to 874 K at ambient pressure in the external-heating DAC. The temperature shifts here were established at ambient pressure and then subtracted from the R_1 line values measured at high P–T. The pressure was calculated based on Ruby2020:[22]

$$P[\mathrm{GPa}] = 1.87(\pm 0.01) \times 10^3 \left(\frac{\Delta\lambda}{\lambda_0}\right) \cdot \left[1 + 5.63(\pm 0.03)\left(\frac{\Delta\lambda}{\lambda_0}\right)\right],$$

where λ_0 is the wavelength of the R_1 line at 694.25 nm at ambient conditions. The maximum pressure uncertainty is ±2.2 GPa at 15.4 GPa and 874 K.[21]

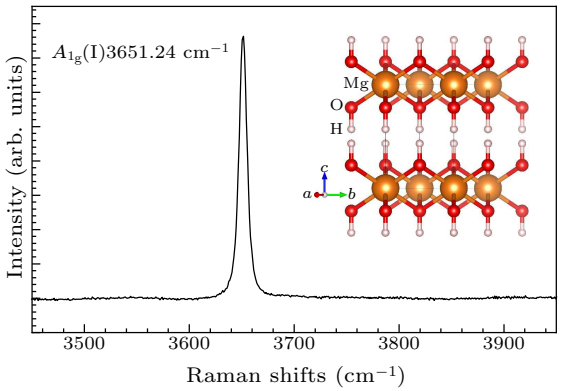

Fig. 1. Crystal structure and Raman spectrum of A_{1g}(I) mode for brucite at ambient conditions.

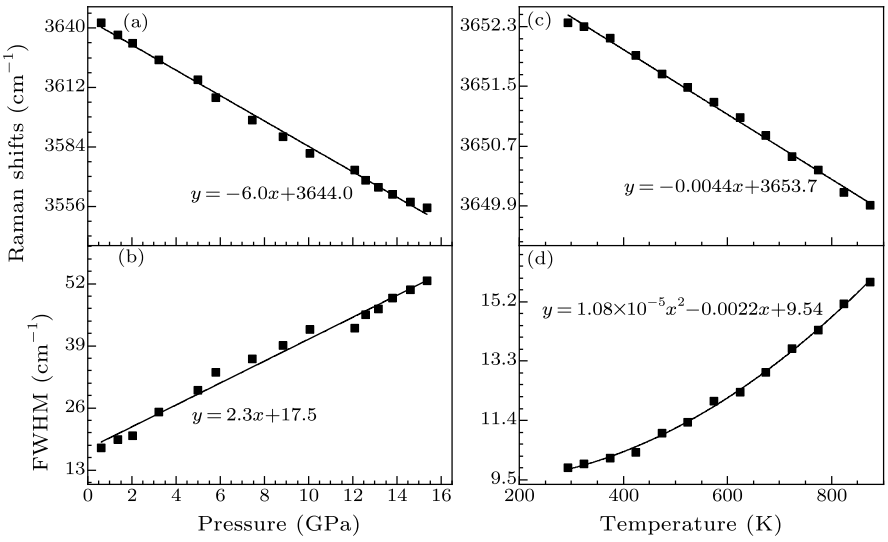

Fig. 2. Pressure and temperature dependences of hydroxyl A_{1g}(I) mode in brucite. Here (a) and (b) show the pressure induced changes of Raman shifts and FWHM at ambient temperature, (c) and (d) are the temperature induced changes of Raman shifts and the FWHM at ambient pressure, respectively.

At room temperature, the Raman spectra of brucite were collected upon decompression from 15.4 GPa to 0.6 GPa. The change of hydroxyl band of brucite at ~3650 cm^{-1} as a function of pressure is plotted in Fig. 2(a). The pressure dependence of the hydroxyl A_{1g}(I) Raman mode is around −6.0(1) cm^{-1}/GPa. It is close to the value of −7 cm^{-1}/GPa reported in the previous research.[8]

Moreover, the pressure evolution of the full widths at half maximum (FWHM) are plotted in Fig. 2(b). The FWHM values of the hydroxyl Raman peak increase with pressure at a rate of 2.3(1) cm^{-1}/GPa. Therefore, Raman shifts of the hydroxyl in brucite decrease with increasing pressure while the corresponding Raman peak width is broadened. The negative pressure dependence of the A_{1g}(I) mode suggests the disorder of H atoms in the hydroxyl of brucite, significantly affecting the strength of intralayer hydrogen bonds,[6,8,23] and the positive pressure dependence of FWHM indicates the anharmonicity from the common softening of phonon modes under pressure.[24]

The Raman spectra of brucite were collected at high temperatures up to 874 K. At ambient pressure, we observed that brucite did not undergo complete dehydration above 674 K as previously reported,[13] likely due to the relatively large grain size and short heat duration at 724–874 K. The temperature dependence of the hydroxyl A_{1g}(I) Raman mode is around −0.44(1) cm^{-1} per 100 K between room temperature and 874 K at ambient pressure [Fig. 2(c)]. The FWHM values increase with increasing temperature [Fig. 2(d)], corresponding to the enhanced anharmonicity from thermal expansion of crystal lattice. In contrast, Zhu *et al.*[25] reported a distinct temperature dependence value of −1.76(10) cm^{-1} per 100 K between 100 to 650 K. The discrepancy could not be readily resolved even with considering the temperature overestimated by ∼50–100 K at high temperatures, which is of less possibility in the two studies. Hence, it is likely a result of the following two aspects: the different temperature ranges and starting $Mg(OH)_2$ samples. The negative temperature dependence is mainly attributed to weakening hydroxyls in brucite.[15]

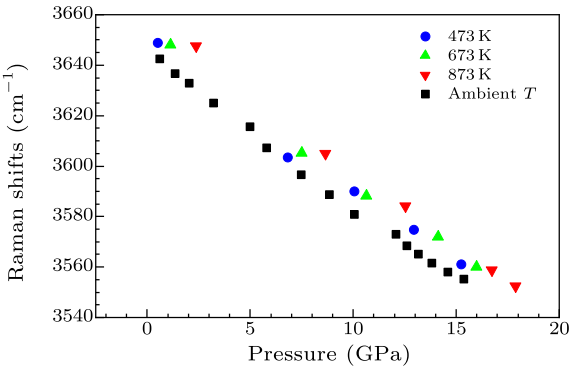

Fig. 3. Pressure-induced Raman shifts of hydroxyl A_{1g}(I) mode at ambient (black squares) and different temperatures.

At 0.2–14.9 GPa, Raman spectra of brucite were taken every 50 K between 300 and 874 K. The pressure evolution of the A_{1g}(I) mode are plotted under different temperatures (Fig. 3). At a given temperature, Raman shifts of the hydroxyl stretching band decrease linearly with increasing pressure at approximately −6 cm^{-1}/GPa. That is, the pressure dependence of hydroxyl band appears insensitive to high temperatures. The linear fitting results are listed in Table 1. The intercepts from different linear fittings follow a positive relationship with increasing temperature, indicating a positive temperature dependence at high pressure. In the previous neutron diffraction research on brucite,[26] with increasing pressure from ambient pressure to 10.9 GPa, the distance between the interlayer O···O configurations decreases from 3.229(2) Å to 2.820(6) Å. Meanwhile, the O–H distance in hydroxyl decreases from 0.919(3) Å to 0.875(8) Å. Therefore, the strength and stability of hydroxyl would increase at elevated pressure. In contrast, Raman shifts of hydroxyl band slightly decreases with increasing temperature at ambient pressure according to this work and the previous study [Fig. 2(c)].[22] The marginally negative temperature dependence likely results from the diminished hydroxyl of brucite at high temperature and ambient pressure. The temperature dependence of the A_{1g}(I) mode changes between ambient and high pressure, suggesting a different mechanism due to the enhanced stability of hydroxyl at high pressure.

Table 1. Linear relationships of pressure and Raman shifts of hydroxyl A_{1g}(I) mode at different temperatures.

Temperature (K)	Slope (cm^{-1}/GPa)	Intercept (cm^{-1})
294	−5.9	3647.8
324	−5.9	3648.2
374	−6.0	3648.2
424	−5.8	3648.1
474	−5.8	3648.9
524	−5.9	3650.1
574	−6.0	3651.6
624	−5.9	3652.1
674	−5.8	3652.4
724	−6.0	3655.3
774	−6.0	3657.5
824	−5.9	3657.4
874	−6.1	3660.4

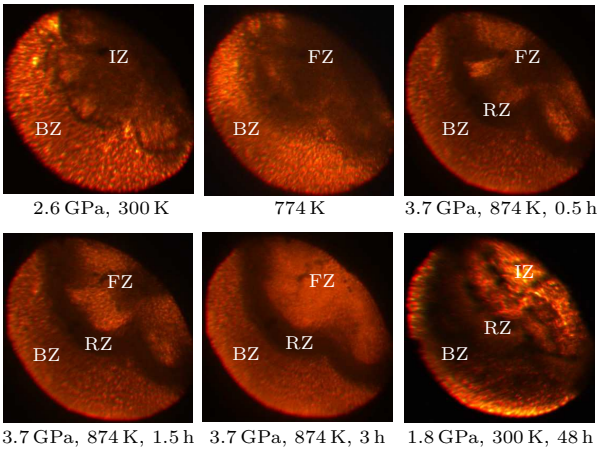

Fig. 4. The changes of sample chamber during high pressure and temperature reaction experiment. There are brucite zone (BZ), reaction zone (RZ) and ice/fluid zone (IZ/FZ) in the chamber. The ice zone melted into fluid at high temperature and recovered at ambient temperature.

Interestingly, the presence of $NaHCO_3$ aqueous solution can make the hydroxyl of brucite unstable at

low pressure and high temperature. The starting materials of brucite powder and $NaHCO_3$ aqueous solution were firstly compressed to 2.6 GPa at room temperature. Liquid aqueous solution transformed into ice phase upon compression.[27] Then the DAC was heated to 874 K where the corresponding pressure increased to 3.7 GPa due to thermal expansion. The optical microscopic images of the sample chamber are illustrated in Fig. 4 upon compression and heating. The sample chamber was divided into the three parts: brucite zone (BZ), reaction zone (RZ), and ice/fluid zone (IZ/FZ). The duration of the heating period lasted for several hours, and Raman measurements were taken on the three zones at simultaneous high P–T conditions (Fig. 5). Raman spectra were also collected upon decompression at room temperature and the quenched sample was recovered for further composition analysis.

There was no Raman signal of CO_3^{2-} or HCO_3^- observed in the brucite zone at ambient conditions due the brucite sample touching the both anvils (black curve in Fig. 5). When the DAC was heated to 874 K, one Raman peak would appear at 1120 cm^{-1} and could be assigned to CO_3^{2-} in the reaction zone (red curve in Fig. 5). When being quenched to room temperature, the two Raman peaks emerged out at 1108 and 1075 cm^{-1} in the ice zone (blue curve in Fig. 5), which could be assigned to CO_3^{2-} and HCO_3^-. This phenomenon may result from the separation of $NaHCO_3$ from the frozen solution. We note that a clear Raman peak at 1096 cm^{-1} evidenced the existence of $MgCO_3$ (green curve in Fig. 5), which was very close to the standard A_{1g}(I) mode of $MgCO_3$ at 1094 cm^{-1} at ambient conditions.[28] The scanned electron microscope (SEM) was used to determine the quenched reaction products (Table 2). Correspondingly, the generation of $MgCO_3$ was confirmed in several spots in the reaction zone (Fig. 4).

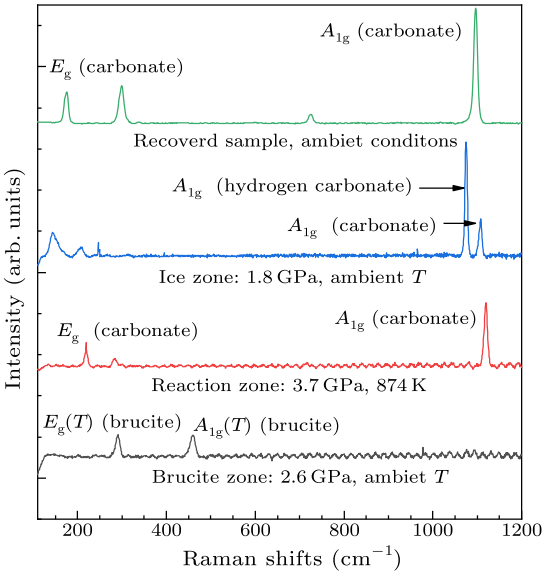

Fig. 5. The change of Raman spectra during high pressure and temperature reaction experiment.

Table 2. Chemical analyses of the recovered sample by SEM.

Elements (at.%)	Spot A	Spot B	Spot C
C	14.32	20.79	
O	63.53	56.45	62.28
Na	4.23	13.31	2.93
Mg	16.91	8.24	33.87
Si	0.24		0.37
Cl			0.33
Fe	0.47	0.79	
Zr	0.31	0.41	
Pt			0.21
Total	100	100	100
Phases	$MgCO_3$, $Mg(OH)_2$, $NaHCO_3$, (Na_2CO_3)	$MgCO_3$, $NaHCO_3$	$Mg(OH)_2$

The above description indicates the following reaction occurring at 3.7 GPa and 674–874 K:

$$Mg(OH)_2 + 2NaHCO_3 \rightarrow MgCO_3 + Na_2CO_3 + 2H_2O.$$

The previous studies[15,16] reported the two reaction stages for the dehydration of brucite under water-saturated conditions at high P–T:

$$Mg(OH)_2 \rightarrow Mg^{2+} + 2OH^-,$$

$$OH^- + H^+ \rightarrow H_2O.$$

The diffusion of H_2O generated in the second stage finally results in the brucite decomposition into periclase at high P–T conditions.[13] However, in HCO_3^--bearing fluids, the second stage is the reaction between OH^- and HCO_3^-. It changes the reaction paths from the dehydration of brucite to the formation of magnesite $MgCO_3$ at the expense of HCO_3^- and CO_3^{2-} ions. The P–T conditions of this reaction are much lower than that of the dehydration of brucite in the transition zone.[29] Due to the relative low solubility, magnesite can crystallize out of aqueous solution. Moreover, magnesite was reported to keep stable until the lowermost mantle P–T conditions.[30] By contrast, subduction fluids may take away most of the calcium carbonate ($CaCO_3$) from oceanic crusts. Previous studies proposed a three-stage carbonate releasing model during oceanic crust subduction based on petrologic evidence from the Dabie–Sulu orogenic belt.[31] The dehydration reaction between brucite and hydrogen carbonate occurs at shallow arc depth (75–

120 km), in which Ca-rich carbonatitic fluids upward to the mantle wedge. When HCO_3^- and CO_3^{2-} ions-bearing subduction fluids mitigate upward into mantle wedge, these ions could react with hydrous minerals (e.g., brucite) to have $MgCO_3$ deposited in the region. Brucite that forms from the serpentinization may not simply decompose into MgO and H_2O, but instead takes part into the formation of Mg-bearing carbonate. That is, most of the dissolved carbonate ions may be retained in the deep mantle through the ion exchange of Mg^{2+} and Ca^{2+} between $CaCO_3$ and Mg-bearing phase. To test this hypothesis, high P–T reactions between carbonate and hydrous phase are imperative to be investigated for further work.

In summary, we have observed the changes in Raman spectra of hydroxyl in brucite under high P–T. The negative pressure dependence of hydroxyl Raman band comes from the disorder of H atoms and the enhancement of intralayer hydrogen-bonding. The negative temperature dependence at ambient pressure is mainly attributed to the diminishing hydroxyl in brucite. The temperature dependences at ambient pressure and high pressure are different, likely associated with the strengthening of hydroxyl bonds at high pressure. On the other hand, brucite is an active component at high P–T conditions of subduction zones. It can react with HCO_3^--bearing fluids originating from the dehydration of carbonates atop the subducted oceanic crusts. These results shed new insights into the interaction between the deep water and carbon cycles.

We appreciate three anonymous reviewers for their constructive suggestions and comments, which are helpful for improvement of the manuscript significantly.

References

[1] Hostetler P, Coleman R, Mumpton F and Evans B 1966 *Am. Mineral.* **51** 75
[2] Wada I and Wang K 2009 *Geochemistry Geophys. Geosystems* **10** Q10009
[3] Kawahara H, Endo S, Wallis S R, Nagaya T, Mori H and Asahara Y 2016 *Lithos* **254–255** 53
[4] Peters D, Pettke T, John T and Scambelluri M 2020 *Lithos* **360** 105431
[5] Moore D E, Lockner D A, Iwata K, Tanaka H and Byerlee J 2001 *US Geological Survey (USGS)* Open-File Report 01–320
[6] Guo X 2016 *Sci. Chin. Earth Sci.* **59** 696 (in Chinese)
[7] Horita J, Santos A M D, Tulk C A, Chakoumakos B C and Polyakov V B 2010 *Phys. Chem. Miner.* **37** 741
[8] Duffy T S, Meade C, Fei Y, Mao H K and Hemley R J 1995 *Am. Mineral.* **80** 222
[9] Fei Y and Mao H K 1993 *J. Geophys. Res.: Solid Earth* **98** 11875
[10] Nagai T, Hattori T and Yamanaka T 2000 *Am. Mineral.* **85** 760
[11] Hermann A and Mookherjee M 2016 *Proc. Natl. Acad. Sci. USA* **113** 13971
[12] Fukui H, Inoue T, Yasui T, Katsura T, Funakoshi K I and Ohtaka O 2005 *Eur. J. Mineral.* **17** 261
[13] Liu C, Liu T and Wang D 2018 *J. Therm. Anal. Calorim.* **134** 2339
[14] Kanzaki M 1991 *Geophys. Res. Lett.* **18** 2189
[15] Liu C, Wang D, Zheng H and Liu T 2017 *Phys. Chem. Miner.* **44** 297
[16] Liu C, Zhang R, Shen K, Liu T, Wen W and Wang D 2018 *Can. Mineral.* **56** 101
[17] Caciagli N C and Manning C E 2003 *Contrib. Mineralogy Petrology* **146** 275
[18] Zigan F and Rothbauer R 1967 *Neues Jahrb Miner. Monatsh* **4** 137
[19] Dawson P, Hadfield C D and Wilkinson G R 1973 *J. Phys. Chem. Solids* **34** 1217
[20] Datchi F, Dewaele A, Loubeyre P, Letoullec R, Godec Y L and Canny B 2007 *High Press. Res.* **27** 447
[21] Raju S V, Zaug J M, Chen B, Yan J, Knight J W, Jeanloz R and Clark S M 2011 *J. Appl. Phys.* **110** 023521
[22] Shen G *et al.* 2020 *High Press. Res.* **40** 299
[23] Kruger M B, Williams Q and Jeanloz R 1989 *J. Chem. Phys.* **91** 5910
[24] Errea I, Rousseau B and Bergara A 2012 *J. Phys.: Conf. Ser.* **377** 012060
[25] Zhu X, Guo X, Smyth J R, Ye Y, Wang X and Liu D 2019 *J. Geophys. Res.: Solid Earth* **124** 8267
[26] Catti M, Ferraris G, Hull S and Pavese A 1995 *Phys. Chem. Miner.* **22** 200
[27] Hemley R J 2000 *Annu. Rev. Phys. Chem.* **51** 763
[28] Farsang S, Facq S and Redfern S A 2018 *Am. Mineral.* **103** 1988
[29] Manning C E 2004 *Earth Planet. Sci. Lett.* **223** 1
[30] Isshiki M, Irifune T, Hirose K, Ono S, Ohishi Y, Watanuki T, Nishibori E, Takata M and Sakata M 2004 *Nature* **427** 60
[31] Shen J, Li S, Wang S, Teng F, Li Q and Liu Y 2018 *Earth Planet. Sci. Lett.* **503** 118